CARBON 49 (2011) 3125–3133

available at www.sciencedirect.com

ScienceDirect

journal homepage: www.elsevier.com/locate/carbon

Differences in cytocompatibility and hemocompatibility between carbon nanotubes and nitrogen-doped carbon nanotubes

M.L. Zhao [a], D.J. Li [a,*], L. Yuan [a], Y.C. Yue [a], H. Liu [b], X. Sun [b]

[a] College of Physics and Electronic Information Science, Tianjin Normal University, Tianjin 300387, China
[b] Department of Mechanical & Materials Engineering, University of Western Ontario, London, ON, Canada

ARTICLE INFO

Article history:
Received 7 January 2011
Accepted 21 March 2011
Available online 29 March 2011

ABSTRACT

The cytocompatibility and hemocompatibility of multiwalled carbon nanotubes and N-doped multiwalled carbon nanotubes grown on carbon papers by chemical vapor deposition were investigated. These materials were characterized using contact-angle measurements, cell- and platelet-adhesion assays, and hemolytic-rate testing, revealing significant effects of nitrogen doping in carbon nanotubes. The results showed that mouse fibroblast cells and mouse adipose-derived stem cells cultured on N-doped multiwalled carbon nanotubes displayed the higher cell-adhesion strength, viability, proliferation, and stretching than those on multiwalled carbon nanotubes without N doping and carbon paper, indicating that N-doped multiwalled carbon nanotubes possessed good cytocompatibility. No toxicity reactions were observed during the culturing period. It also displayed the lowest hemolytic rate.

1. Introduction

Carbon nanotubes (CNTs) are well-ordered, all-carbon, hollow graphitic nanomaterials with a high aspect ratio, lengths ranging from several hundred nanometers to several micrometers and diameters ranging from 0.4 to 2 nm for single-walled CNTs (SWCNTs) to hundreds of nanometers for coaxial multiwalled CNTs (MWCNTs) [1–3]. Bioapplications of CNTs have been predicted and explored since the discovery of these one-dimensional carbon allotropes. Owing to their unique properties and potential applications in a variety of biomedical and biological systems and devices, significant progress has been made in overcoming several fundamental and technical barriers to bioapplication, in particular, barriers associated with the aqueous solubility and biocompatibility of CNTs and the design and fabrication of prototype biosensors [4–6].

Recently, the investigation of CNTs in biomedical applications has focused primarily on preventing nonspecific protein adsorption [7,8] and identifying particular proteins [9] by surface modification, as well as on promoting cell growth as a culture medium by utilizing the uniquely individual shapes and electrical properties of CNTs [10]. The advantages of CNTs include lower toxicity and their ability to maintain their intrinsic cytoimmunity function [11–13].

The modification of CNTs by the inclusion of nitrogen has been suggested to have positive effects on their biocompatibility and structural properties; however, despite promising studies of CNTs for biomedical applications, N-doped multiple-walled CNTs (N-MWCNTs) have not been used in biomedical studies to date. N-MWCNTs consist mainly of carbon and nitrogen, with minor amounts of hydrogen and oxygen. Like CN_X [14–18], N-MWCNTs should be an excellent candidate for applications as biocompatible materials in

* *Corresponding author:* Fax: +86 22 23766519.
E-mail addresses: dli1961@126.com, dejunli@mail.tjnu.edu.cn (D.J. Li).
0008-6223/$ - see front matter © 2011 Elsevier Ltd. All rights reserved.
doi:10.1016/j.carbon.2011.03.037

biomedical implants because of their desirable properties, such as high chemical stability and a chemical composition that includes only elements that are biologically compatible and found in living tissue, implying that N-MWCNTs may possess excellent biocompatibility. However, there have been few studies on the biocompatibility of N-MWCNTs, especially in hemocompatibility investigations (e.g., hemolysis, platelet-adsorption, and cell-adhesion assays) in the current literature. Additional investigations of cell adhesion, growth, blood–protein adsorption, and toxic effects on animals are needed. The aim of this work was to compare the biocompatibilities of MWCNTs and N-MWCNTs by investigating hemolysis, platelet adsorption and cell adhesion in cultures with both materials.

2. Experimental details

2.1. Preparation of MWCNTs and nitrogen-doped MWCNTs

The syntheses of MWCNTs and N-MWCNTs were carried out using a chemical vapor deposition (CVD) system that has three main components: an aerosol generator, a modified quartz chamber placed in a furnace and, a gas trap for the exhausting gases. The method is based on the decomposition of an aerosol consisting of a liquid hydrocarbon source and a volatile catalyst for MWCNT formation. First, a 30 nm Al layer was sputtered onto carbon paper, which was loaded into a ceramic boat and placed inside the chamber. There were three argon inlets and one hydrogen inlet in this system; one argon inlet allows this carrier gas to flow through the hydrocarbon solution and deliver it as an aerosol into the reaction chamber. Two additional argon inlets enable the dilution of the aerosol mixture. Hydrogen is also introduced into the reaction chamber from a hydrogen inlet. The solution used as the carbon feedstock is placed inside a sonication generator and held at room temperature by cooling water during the synthesis. Here, m-xylene was used as the carbon feedstock for the growth of N-MWCNTs, and acetonitrile was used as the combined carbon and nitrogen feedstock for the growth of N-MWCNTs. The thickness of MWCNTs or N-MWCNTs substrates was roughly 50–70 μm.

2.2. Cell-adhesion assays

Mouse fibroblast cells (L929) and mouse adipose-derived stem cells (ADSCs) were used to investigate the cytocompatibilities of MWCNTs, N-MWCNTs and carbon paper. The mouse ADSCs were isolated from the inguinal fat pad of 300–600 g guinea pigs in an aseptic environment. Freshly isolated ADSCs were carefully washed with the same volume of phosphate buffer to remove the blood and large vessels. An equal volume of 0.075% collagenase I solution was added, and the cells were digested for 90 min with slight shaking. The ADSCs were cultured in essential medium with a low-glucose Dulbecco's Modified Eagle's Medium (DMEM) supplemented with 10% fetal calf serum, 1% penicillin (10,000 units/ml) and 1% streptomycin solution (10,000 μg/ml). Finally, a single-cell suspension was prepared by centrifuging the cultures twice at 1300 rpm for 15 min. The mouse fibroblast cells L929 were cultured in essential medium with DMEM supplemented with 10% fetal calf serum, 1% penicillin and 1% streptomycin solution (Hyclone shv30010).

The two types of cells prepared above were both grown as monolayers in 24-well culture plates with and without materials of carbon papers, MWCNTs and N-MWCNTs at 37 °C under 5% CO_2/95% air, and the medium was changed every 2 days. After 1–7 days in the incubator (culture intervals of 1, 1.5, 2, 3, 5, and 7 days), the medium was removed and the cell monolayer was washed several times with PBS and then fixed in methanol for enumeration. Trypan blue dye assay was used to count alive and dead cell numbers after different incubation days in order to confirm the viability of both cells. ADSCs and L929 cells in 24-well culture plates without materials were used as the control group. Each sample contained at least 1×10^4 unfixed ADSCs cells, and the inoculum density of mouse fibroblast cells was 2×10^4 cells/ml. Before both cells seeding on the materials, the percentage of the alive cell numbers was over 95%.

2.3. Platelet-adhesion and hemolytic-rate experiments

Platelet-adhesion testing was performed to investigate the morphology, quantity and aggregation of the adherent platelets on the surfaces of the materials. Anticoagulated blood was prepared from 20 ml healthy rabbit blood plus 1 ml 2% potassium oxalate. Anticoagulated blood solution was obtained by adding 10 ml normal saline (NS) to 8 ml anticoagulated blood. A 5 cm^2 piece of carbon paper, MWCNTs or N-MWCNTs samples were placed in each Erlenmeyer flask in the sample group and washed three times with NS. The same numbers of Erlenmeyer flasks with either 5 ml NS or distilled water was used as negative and positive control groups, respectively. After heating in water bath at 37 ± 1 °C for 30 min, 0.05 ml of anticoagulated blood solution was injected into the flasks of all three groups, which were then shaken and heated to 37 ± 1 °C for 60 min. The supernatant was removed by 15 min centrifugation, and the optical density (OD) at 545 nm was measured with a spectrophotometer. OD values were related to the concentration of free hemoglobin in the supernatant due to broken red blood cells.

Two pieces of carbon paper, two pieces of MWCNTs and two pieces of N-MWCNTs with identical areas of 1 cm^2 were placed in 24-well culture plates as sample groups. One hundred and forty glass balls 0.5 mm in diameter (the total surfaces area of 140 glass balls were about 1 cm^2), with and without a coating of methylsilicone oil, were placed in the 24-well culture plates as negative and positive control groups, respectively. The thickness of methylsilicone oil was roughly dozens of micron. Healthy rabbit blood was placed into contact with all three groups. After 15–60 s of contact, blood samples were removed from the 24-well culture plates and then blended with 1% ethylenediamine tetraacetic acid (EDTA) at 9:1; a platelet-preservative solution was then added to prevent blood coagulation. After diluted using mixture of EDTA and platelet-preservative solution, the blood samples were dropped on the blood cell counting plate to count platelet numbers for identifying the platelet adhesion of three groups.

2.4. Contact-angle, SEM, XPS, and TEM analysis

A CAM 200 optical contact-angle inclinometer (Nunc, Finland) was used to measure the contact angle of the samples. Here, 20 μl of distilled water was dropped onto the material surfaces, and the contact angle was then determined using the dedicated software.

The morphology of the MWCNTs and N-MWCNTs was examined with a field-emission scanning electron microscope (FESEM, Hitachi S-4800 or Quanta 200) operated at 5.0 kV. The scanning electron microscope (SEM), combined with an optical microscope, was also employed to observe cell or platelet morphology and stretching on the surfaces of the carbon paper, MWCNTs, and N-MWCNTs. The detailed morphologies and incorporated nitrogen concentrations of the MWCNTs and N-MWCNTs were characterized using a Philips CM10 transmission electron microscope (TEM) operated at 80 kV and a Kratos Axis Ultra Al (alpha) X-ray photoelectron spectroscope (XPS) operated at 14 kV.

3. Results and discussion

3.1. Morphological and nitrogen atomic concentrations of the carbon paper, MWCNTs, and N-MWCNTs

Fig. 1a–c shows SEM images of the carbon paper, MWCNTs and N-MWCNTs, respectively. From Fig. 1b and c, it can be seen that the carbon fibers are completely covered by nanotubes at high density.

HRTEM images of MWCNTs and N-MWCNTs are shown in Fig. 2. The tubular structure of these two samples is seen in these figures. Their outer diameters are approximately 30–40 nm, and the wall thicknesses are both around 10 nm. Amorphous carbon is observed on the surfaces of both types of nanotubes (shown by black arrows). It can be seen that the graphite layers of the MWCNTs are generally parallel to each other with small curvature, while N-MWCNTs shows a bamboo-like structure, in which a interlinks are observed within the tubes (shown by white arrow). The crystallinity decrease when nitrogen atoms were doped into the tubes which was discussed in detail elsewhere [19]. The N atomic concentration present in the N-MWCNTs was estimated from the peak-area ratio of the nitrogen and carbon peaks in the XPS spectrum, which has been discussed in detail previously [19].

3.2. Contact-angle measurements

Table 1 shows the results of water-contact-angle testing. Generally speaking, where a contact angle is larger than 65°, this kind of surface is defined as hydrophobic. Table 1 indicates that the water-contact angles of all the three materials were larger than 125°, evidencing their hydrophobic properties. The N-MWCNTs displayed slightly higher hydrophobicity than the MWCNTs.

3.3. Cellular morphology and viability of mouse-fibroblast cells and ADSCs

Before any material is used for medical purposes, it must pass a series of tests in terms of its biocompatibility. In vitro cell culture in controlled conditions is one of the most often-used methods. In this work, we chose mouse-fibroblast cells for

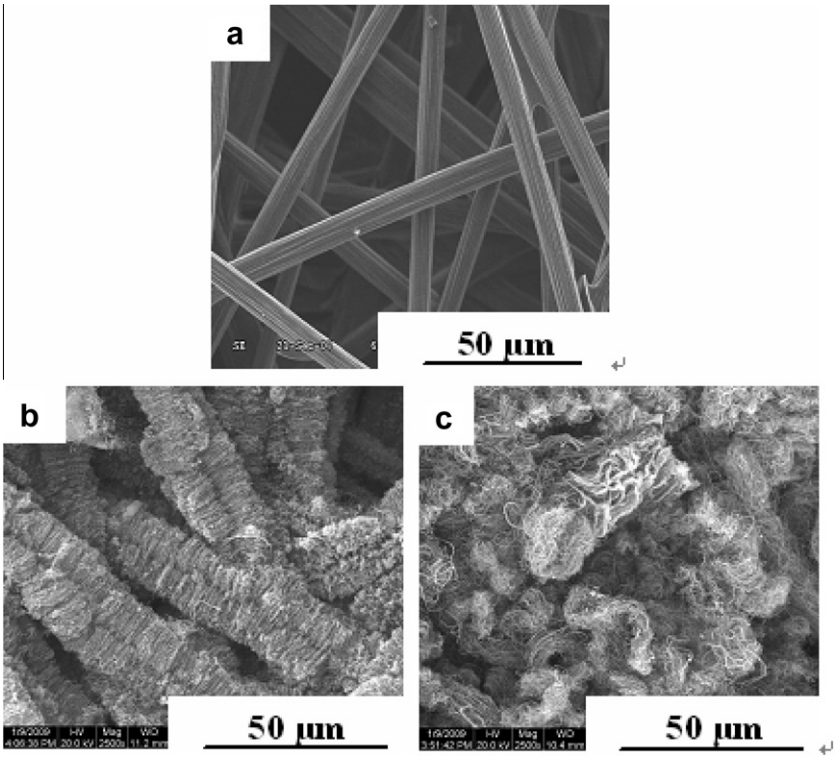

Fig. 1 – SEM images of (a) carbon paper, (b) MWCNTs, (c) N-MWCNTs.

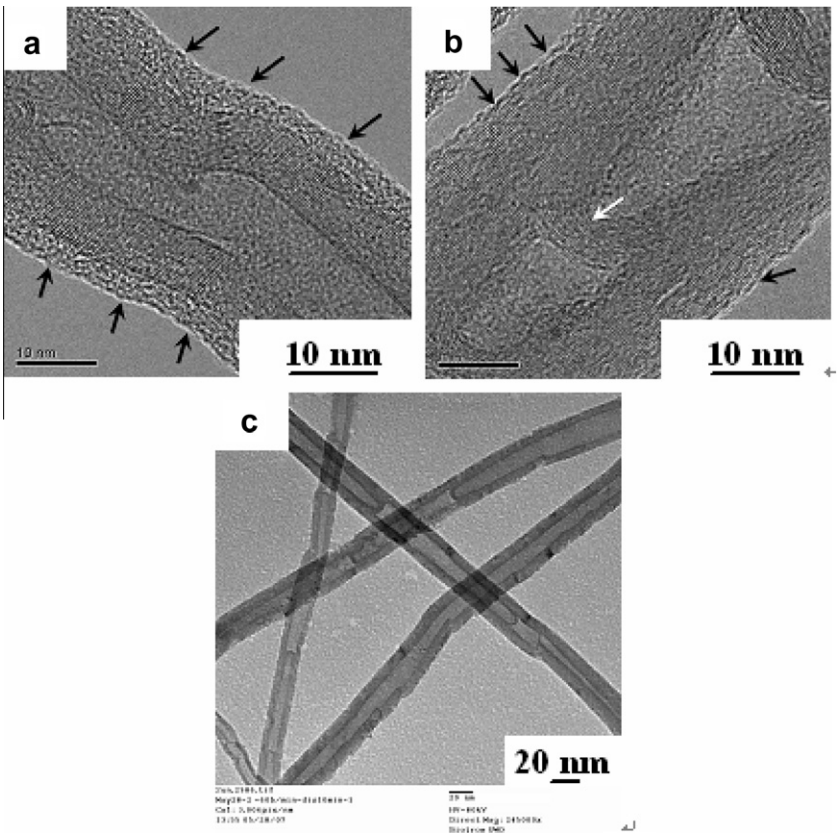

Fig. 2 – HRTEM images of (a) MWCNTs, (b, c) N-MWCNTs.

direct contact measurements and investigation of cell viability at 1, 1.5, 2, 3, 5 and 7 days through a biological inversion microscope. Trypan blue dye was used to count alive and dead cell numbers. Fig. 3 shows alive L929 mouse-fibroblast cell numbers on the surfaces of the different materials with incubation days. Each values in this figure represent the mean ± SD for five measurements. Each experiment was performed three times. From 1 to 3 days, the concentration of control group increased gradually, but after 5 days, the cell numbers reduced gradually. However, the cell concentrations on carbon paper, MWCNTs and N-MWCNTs sustained increases from 1 to 7 days, despite lower cell numbers adhering to the three materials than that in the control group for the first few days. Good cell viability on the surfaces of the three materials indicates that the large network structure provides a better growth environment for cell viability. From 1 to 3 days, no dead cells were observed under the microscope about all the samples. After 7 days incubation, the percentage of the dead cell numbers from N-MWCNTs was the lowest value of 11%, whereas the percentage of the dead cell numbers from control group was up to over 21%. Interestingly, among these materials, the N-MWCNTs displayed the strongest cell viability.

Table 1 – Results of water-contact-angle testing of the three materials.

Material contact angle (°)	Carbon paper	MWCNTs	N-MWCNTs
Height test	126.87	131.13	137.64
Angle test	126.00	131.75	138.75
Average value	126.44	131.44	138.20

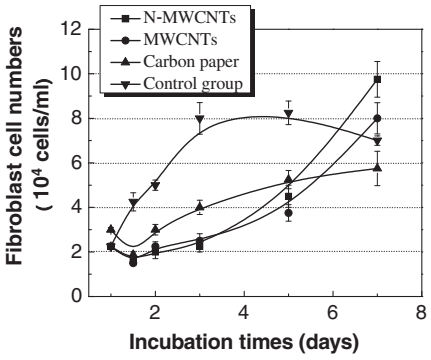

Fig. 3 – L929 mouse-fibroblast cell numbers on the surfaces of the different materials *vs.* incubation time.

This result is probably related to the contribution of nitrogen functional groups to cellular tissues and the three-dimensional configuration of the N-MWCNTs, which offers a much larger substrate area for cell growth and proliferation.

The SEM images in Fig. 4 show the morphology of mouse-fibroblast cells fixed on the surface of carbon paper, N-MWCNTs and MWCNTs after the incubation at different magnifications. Compared with the irregular, spindly cells on the carbon paper (Fig. 4a and b), typical triangular cells adhered to the surface of the MWCNTs and N-MWCNTs (Fig. 4c–f). This

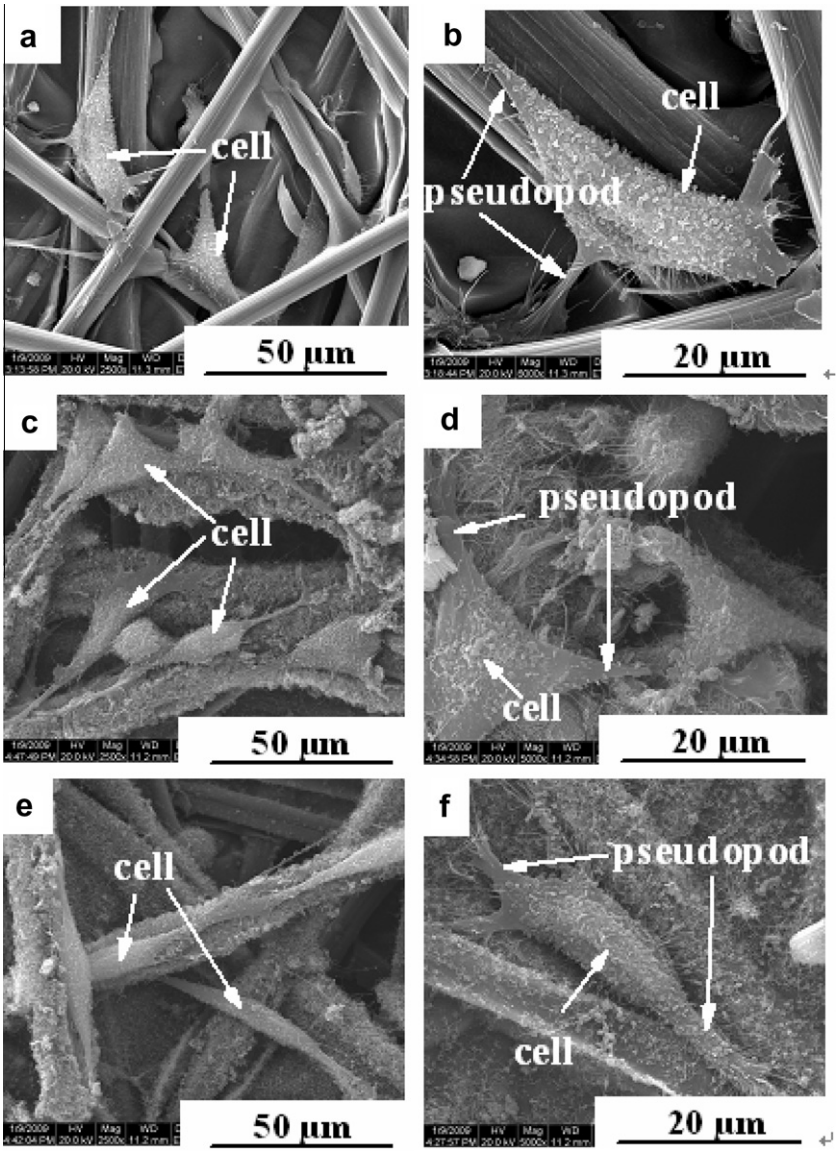

Fig. 4 – SEM images of mouse-fibroblast cells fixed on the surfaces of (a, b) carbon paper, (c, d) N-MWCNTs, and (e, f) MWCNTs.

suggests that the MWCNTs and N-MWCNTs provide better conditions for the cellular stretching and pseudopod spreading, which may be related to their rough surfaces and three-dimensional configurations. In general, rough surfaces can increase the contact area of cells with the materials and promote the cell-wetting surface [20,21], enhancing cell adhesion. In addition, cell-adhesion strength can also be increased when small nicks or other microstructures exist on a material surface, as the adhesion and growth of cells are generally along the surface of a fiber or notch to provide contact guidance [22–24]. Compared with carbon paper, therefore, the MWCNTs and N-MWCNTs possess rougher surfaces and larger surface areas, leading to higher cell-adhesion strengths. It is clear from Fig. 4c and e that the fibroblast cells spread flat, completely covering the N-MWCNT surface but not the MWCNT surface. This is possibly because nonspecific binding between nitrogen in the N-MWCNTs and cell-surface proteins enhanced cell adhesion and growth on the N-MWCNTs.

Guinea-pig inguinal adipose tissue was digested by collagenase treatment and then the isolated ADSCs were plated on 24-well culture plates. At the first day after plating, the ADSCs adhered to the plastic surfaces of tissue-culture plates, displaying a small population of polygonal or spindle shapes (Fig. 5a). At 72 h after inoculation, the cells had propagated and spread rapidly in vitro, significantly adhering to the surface of the culture plates and extending long pseudopodia, which were interconnected to form a homogeneous fibroblast-like morphology, as shown in Fig. 5b. The spindles as well as granules around the nucleus also increased gradually, which shows the state of ADSC division.

To investigate ADSC viability on the three materials, the cell numbers on the carbon paper, MWCNT, and N-MWCNT samples were counted after 1–7 days of incubation, as shown in Fig. 6. Values in this figure represent the mean ± SD for five measurements. Each experiment was performed three times. It can be seen in the figure that the cell number of the control group increased gradually from 1 to 7 days; a large number of

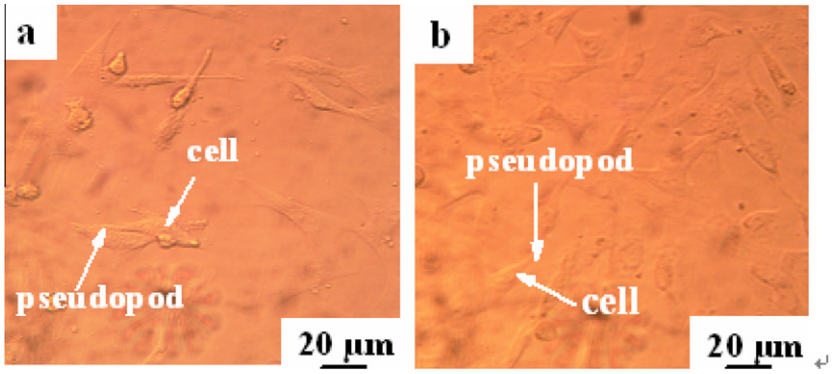

Fig. 5 – Optical micrographs of ADSCs (a) 24 h and (b) 72 h after inoculation.

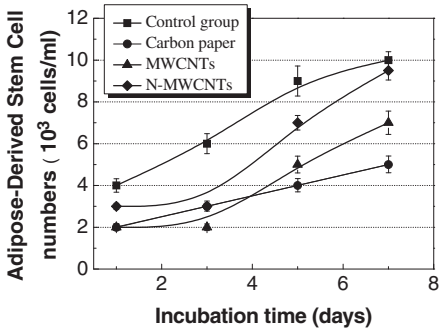

Fig. 6 – ADSC numbers on the surfaces of different materials *vs.* incubation time.

cells divided over time. After 5 days, the cell numbers of the control group increased slowly. Compared with the low number and low viability of the cells on the carbon paper, high cell numbers and rapid proliferation were observed on the MWCNTs and N-MWCNTs. The cell growth rates were in the following order: MWCNTs-N > MWCNTs > carbon paper.

Indeed, Fig. 6 does not show a significant difference in cell numbers between the control group and the N-MWCNT on day 7. Because 24-well culture plate, which was employed as the control group and standard cell culture plate, is one of the best materials for cell viability and proliferation, as a comparable to 24-well culture plates in cell numbers, N-MWCNT displays better cell viability than MWCNTs and carbon paper. Besides, the ADSCs implanted on the N-MWCNTs still indicated a rapid increase trend in numbers after 7 days. Therefore, it is providing further evidence of the good cytocompatibility of the N-MWCNTs.

3.4. *Platelet-adhesion and hemolytic rates*

Methylsilicone oil has excellent anticoagulant activity, but glass balls cause coagulation, so we choose the two as reference groups. The platelet-adhesion rate of a material can be represented as follows: Platelet adherent rate$(\%) = \frac{A-B}{A} \times 100\%$, where A is the total number of platelets and B is the number of platelets remaining in the blood after the platelet-adhesion testing. A larger B value indicates lower platelet adhesion on the materials. Table 2 gives the platelet adhesion rates of different materials including the blank and the negative and positive control groups of the glass balls with or without methylsilicone oil, respectively. Values in this table represent the mean ± SD for five measurements.

It is clear that the platelet-adhesion rates of the carbon paper, N-MWCNTs and MWCNTs were comparable to or lower than that of the negative control group, which indicates their good anticoagulation properties and acceptable clinical use. MWCNTs showed the lowest platelet-adhesion rate among all the materials. Thrombus formation involves a complex cascade of biochemical reactions and path signaling biological processes [25], with the biochemical, electrochemical and physical behavior of individual blood components, such as coagulation factors, thrombocytes and selected enzymes coming into contact with a sample surface. It is believed that fibrinogen is a principal clotting factor among those blood components [26], and the adsorption to the biomaterial surface then transformation to fibrin of fibrinogen is of significance in thrombus formation. The properties of the biomaterial surface like surface energy, roughness, surface hydrophobicity, zeta potential, etc. affect the hemocompatibility of the biomaterial [27,28]. However, it is difficult to

Table 2 – Average numbers and adhesion rates of platelets on the different materials.

Material	Average numbers of platelets	Platelet adhesion rate (%)
Blank group (cell culture plate)	347.5	–
Negative control group (glass ball with methylsilicone oil)	281	19.14
Positive control group (glass ball without methylsilicone oil)	72.5	79.13
Carbon paper	268	22.87
N-MWCNTs	279.5	19.57
MWCNTs	323.5	6.9

demonstrate the influence of each factor. Although the mechanisms of hemocompatibility of carbon materials with various ratio of sp^3 C to sp^2 C are not clear yet, numerous studies imply that the hemocompatibility of carbon materials is influenced by the ratio of sp^3 to sp^2, not by the absolute sp^3 or sp^2 content [29–31]. Fibrinogen has an electronic structure similar to semiconductor. Its energy gap is 1.8 eV [32], and the valence band and conduction band are at 0.9 eV below and above the Fermi level, respectively [26]. When the energy gap of the biomaterial reaches 2.8 eV, the penetration factor is in the minimum as the Fermi level of the biomaterial equals to that of fibrinogen, the biomaterial is the best in the hemocompatibility [26]. Therefore, there is an optimum band gap, in other words, a suitable ratio of sp^3 C to sp^2 C in the carbon nanotubes, can provide the optimum density of charge to promote the hemocompatibility. The more proper sp^3 to sp^2 ratio in MWCNTs may be one of the reasons for the lowest platelet-adhesion rate.

Platelet adhesion on the carbon paper, MWCNTs, and N-MWCNTs was observed by SEM. A dense fibrin network containing randomly distributed platelets was seen on the surface of the carbon paper (Fig. 7a). Conversely, there were few fibrin networks or platelet aggregations observed on the surface of the N-MWCNTs and MWCNTs after exposure to platelet-rich plasma, as shown in Fig. 7b and c, indicating insignificant thrombosis on both surfaces. Platelet adhesion and activation are the inevitable results of the interaction of blood and materials. When blood contacts a material, fiber protein, factor XII and other plasma proteins first competitively adsorb on the surface of the material for ~5 s; platelets then adhere to the plasma-protein coated materials. Among the plasma proteins, fibrinogen is regarded as the key protein that triggers platelet adhesion, activation and aggregation. Subsequently, coagulation factors are released, initiating the coagulation cascade and the eventual formation of a thrombus [33]. Conformational change of the adsorbed fibrinogen layer plays an important role in mediating the platelet response to a material surface. On the N-MWCNTs, due to the positively charged nitrogen ions, the reorganization of Hfg upon attachment appears to favor subsequent binding of the platelet glycoprotein GPIIb/IIIa epitopes. Fibrinogen is a required step for platelet adhesion to surfaces as binding of the GPIIb/IIIa receptor, the ligand-inducing binding site (LIBS), on the membrane of platelets forms a specific bond with the receptor-inducing binding site (RIBS) on fibrinogen, whereby the latter becomes available when it reveals its RIBS sequence for specific interaction with the former when undergoing conformational changes [34]. Because the chemistry of MWCNTs and graphite are similar, and the graphite shows the negatively charge due to each carbon atom will emit an electronic, the surface of MWCNTs exhibited lower fibrinogen adsorption as well as platelet adhesion. Similar observations have been reported by other researchers, wherein the conversion of adsorbed fibrinogen to fibrin was comparatively ineffective on the negatively charged surface of self-assembled monolayers (SAMs) containing a carboxyl-terminated group [35]. This may explain the results of our experiments.

The hemolytic rate was calculated from the average OD value of the materials and control groups using the following formula: Platelet adherent rate$(\%) = \frac{A-B}{C-B} \times 100\%$, with A, B, and C being the OD values of, respectively, the test materials, the negative control group, and the positive control group (H_2O). According to the YY/T0127.1 standard, a hemolytic rate below 5% is acceptable [36,37]. Table 3 lists the hemolytic-rate results of the different materials.

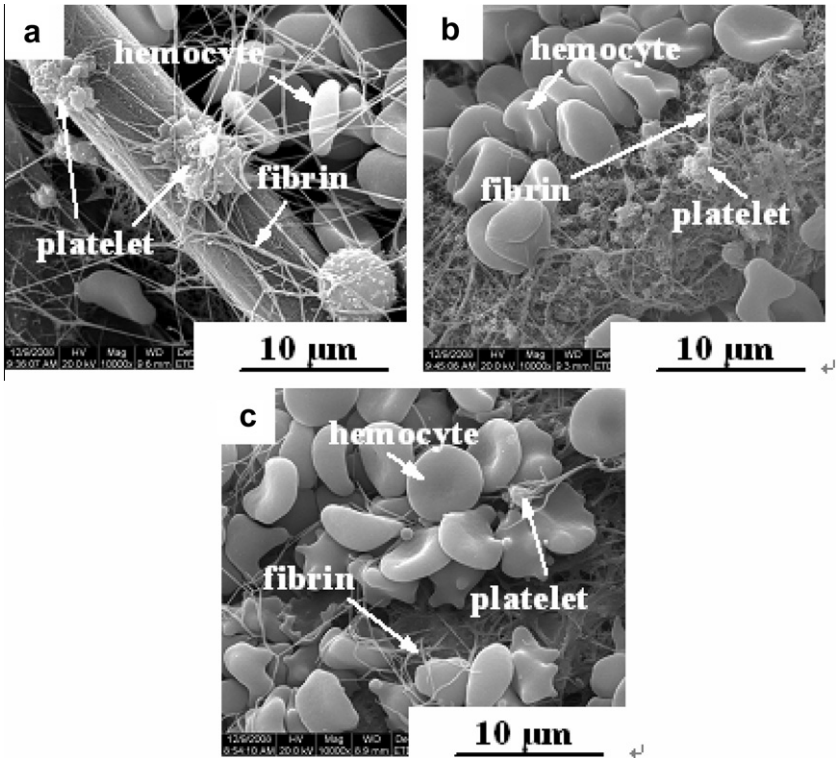

Fig. 7 – SEM images of the platelet-adhesion testing for (a) carbon paper, (b) N-MWCNTs, and (c) MWCNTs.

Table 3 – Hemolytic rates of the different materials.

Materials	OD value 1	OD value 2	OD value 3	Average of OD value	Hemolytic rate (%)
Negative control group	0.009	0.010	0.014	0.011	–
H_2O	0.242	0.240	0.244	0.242	–
Carbon paper	0.014	0.013	0.016	0.0143	1.43
MWCNTs	0.014	0.013	0.015	0.014	1.3
N-MWCNTs	0.014	0.011	0.014	0.013	0.87

In these tests, we found that the red blood cells were at the bottom, and a clear, colorless supernatant of the Erlenmeyer flask containing the negative control group. However, the upper layer of the flask containing the positive control group (H_2O) was a red, cloudy supernatant because of a large amount of hemoglobin released from broken red blood cells due to osmotic shock. The carbon paper, MWCNTs and N-MWCNTs performed as well as the negative control group. The hemolytic rates of both the MWCNTs and N-MWCNTs were lower than the standard value of 5%, meaning that both MWCNTs and N-MWCNTs are classified as nonhemolytic materials. Compared with MWCNTs, N-MWCNTs had a lower hemolytic rate, with the lowest value of 0.87%. The interaction of N-containing functional groups with blood tissues thus seemed to have a positive effect on hemocompatibility.

4. Conclusions

In this study, mouse-fibroblast cells (L929) and mouse ADSCs cells adhered to the MWCNTs and N-MWCNTs to form a rapidly expanding population of polygonal cells. Notably, N-MWCNTs displayed the highest cell-adhesion strength, cell viability, cell proliferation, cell stretching, and pseudopod spreading due to the contribution of N-containing functional groups to cell tissues as well as the three-dimensional configuration and rougher surface morphology of the material, which supported its good cytocompatibility. N-MWCNTs also displayed a lower hemolytic rate (0.87%) and inhibited platelet adhesion and thrombus formation. This study demonstrated the good biocompatibility of N-MWCNTs as promising and effective biomedical material that might have clinical applications in the future, in particular as substrates for the tissue regeneration.

Acknowledgements

The authors would like to thank professor C.J. Zhu, Tianjin Normal University for important discussion and help of this work. This work was supported by National Natural Science Foundation of China (11075116), the Open Research Fund of the State Key Laboratory of Bioelectronics, Southeast University (2010-2012), and the Key Laboratory of Beam Technology and Material Modification of the Ministry of Education, Beijing Normal University (201014), China.

REFERENCES

[1] Iijima S. Helical microtubules of graphitic carbon. Nature 1991;354(6348):56–8.

[2] Dresselhaus MS, Dresselhaus G, Eklund PC. Science of fullerenes and carbon nanotubes. New York: Academic Press; 1996.

[3] Chor YT, Gu HG, Leong WS, Yu HY, Li HQ, Heng BC, et al. Cellular behavior of human mesenchymal stem cells cultured on single-walled carbon nanotube film. Carbon 2010;48(4):1095–104.

[4] Alla LA, Shan WQ, Pavel B, Brad LU, Adam RR, Susan JM, et al. Single-walled carbon nanotubes dispersed in aqueous media via non-covalent functionalization: effect of dispersant on the stability, cytotoxicity, and epigenetic toxicity of nanotube suspensions. Water Res 2010;44(2):505–20.

[5] Lin Y, Taylor S, Li HP, Shiral FKA, Qu LW, Wang W, et al. Advances toward bioapplications of carbon nanotubes. J Mater Chem 2004;14(4):527–41.

[6] Kalbacova M, Kalbac M, Dunsch L, Kataura H, Hempel U. The study of the interaction of human mesenchymal stem cells and monocytes/macrophages with single-walled carbon nanotube films. Phys Stat Sol 2006;243(13):3514–8.

[7] Cenni E, Granchi D, Arciola CR, Ciapetti G, Savarino L, Stea S, et al. Adhesive protein expression on endothelial cells after contact in vitro with polyethylene terephthalate coated with pyrolytic carbon. Biomaterials 1995;16(16):1223–7.

[8] Cui FZ, Li DJ. A review of investigations on biocompatibility of diamond-like carbon and carbon nitride films. Surf Coat Technol 2000;131(1–3):481–7.

[9] Heon WC, Reinhold HD, Lee SC, Lee KR, Kyu HO. Characteristic of silver doped DLC films on surface properties and protein adsorption. Dia Rel Mater 2008;17(3):252–7.

[10] Smart SK, Cassady AI, Lu GQ, Martin DJ. The biocompatibility of carbon nanotubes. Carbon 2006;44(6):1034–47.

[11] Wang JG, Jiang N. Blood compatibilities of carbon nitride film deposited on biomedical NiTi alloy. Dia Rel Mater 2009;18(10):1321–5.

[12] Pulskamp K, Diabate S, Krug HF. Carbon nanotubes show no sign of acute toxicity but induce intracellular reactive oxygen species in dependence on contaminants. Toxicol Lett 2007;168(1):58–62.

[13] Dumortier H, Lacotte S, Pastorin G, Marega R, Wu W, Bonifazi D, et al. Functionalized carbon nanotubes are non-cytotoxic and preserve the functionality of primary immune cells. Nano Lett 2006;6(7):1522–7.

[14] Quirós C, Núñez R, Prieto P, Elizaldea E, Fernándezb A, Schubertc, et al. Tribological and chemical characterization of ion beam-deposited CNx films. Vacuum 1999;52(1–2):199–201.

[15] Galeano ODS, Vargas S, López CLM, Ospina R, Restrepo PE, Arango PJ. Substrate temperature influence on the trombogenicity in amorphous carbon nitride thin coatings. Appl Surf Sci 2010;256(24):7484–9.

[16] Su XW, Song HW, Cui FZ, Li WZ, Li HD. Formation of β-C_3N_4 grains by nitrogen-ion-beam-assisted deposition. Surf Coat Technol 1996;84(1–3):388–97.

[17] Song HW, Cui FZ, He XM, Li WZ, Li HD. Carbon nitride films synthesized by NH_3-ion-beam-assisted deposition. Condens Matter 1994;6(31):6125–30.

[18] Fuminori F, Ogata K. Formation of carbon nitride films by means of ion assisted dynamic mixing (IVD). Meth Appl Phys 1993;32(13):420–3.
[19] Liu H, Zhang Y, Li RY, Sun XL, Sylvain D, Hakima AR, et al. Structural and morphological control of aligned nitrogendoped carbon nanotubes. Carbon 2010;48(5):1498–507.
[20] Kenichi M, Frank XW, Masao Y, Takashi I, John AJ. The attachment and growth behavior of osteoblast-like cells on microtextured surfaces. Biomaterials 2003;24(16):2711–9.
[21] Chor YT, Gu HG, Leong WS, et al. Cellular behavior of human mesenchymal stem cells cultured on single-walled carbon nanotube film. Carbon 2010;48(4):1095–104.
[22] Curtis A, Wikinsion C. Topographical control of cells. Biomaterials 1997;18(24):1573–83.
[23] Puja C, Ajit S, Anju S. Cisplatin primes murine peritoneal macrophages for enhanced expression of nitric oxide, proinflammatory cytokines, TLRs, transcription factors and activation of MAP kinases upon co-incubation with L929 cells. Immunobiology 2009;214(3):197–209.
[24] Ana LE, Julio CCS, Humberto T, Morinobu E, Juan PL, Mauricio T. Viability studies of pure carbon- and nitrogen-doped nanotubes with *entamoeba histolytica*: From amoebicidal to biocompatible structures. Small 2007;3(10):1723–9.
[25] Bark N, Földes-Papp Z, Rigler R. The incipient stage in thrombin-induced fibrin polymerization detected by FCS at the single molecule level. Biochem Biophys Res Commun 1999;260(1):35–41.
[26] Liu Y, Li ZY, He ZH, et al. Structure and blood compatibility of tetrahedral amorphous hydrogenated carbon formed by a magnetic-field-filter plasma stream. Surf Coat Technol 2007;201(15):6851–6.
[27] Leng YX, Chen JY, Yang P, et al. Mechanical properties and platelet adhesion behavior of diamond-like carbon films synthesized by pulsed vacuum arc plasma deposition. Surf Sci 2003;531(2):177–84.
[28] Okpalugo TIT, Ogwu AA, Maguire PD, et al. Platelet adhesion on silicon modified hydrogenated amorphous carbon films. Biomaterials 2004;25(2):239–45.
[29] Baurschmidt P, Schaldach M. Alloplastic materials for heart-valve prostheses. Med Biol Eng Comput 1980;18(4):496–502.
[30] Gu HQ. Biomedical materials. Tianjin: Science and Technology Translation Press; 1993 [in Chinese].
[31] Chen JY, Wang LP, Fu KY, et al. Blood compatibility and sp^3/sp^2 contents of diamond-like carbon (DLC)synthesized by plasma immersion ion implantation-deposition. Surf Coat Technol 2002;156(1–3):289–94.
[32] Baurschmidt P, Schaldach M. The electrochemical aspects of the thrombogenicity of a material. J Bioeng 1977;1(1):261–78.
[33] Feng L, Andrade JD. Proteins at interfaces II: fundamentals and applications. In: Horbett TA, Brash JL, editors. Structure and adsorption properties of fibrinogen. Washington, DC: American Chemical Society; 1995.
[34] Harrison P. Progress in the assessment of platelet function. Brit J Haematol 2000;111:733–44.
[35] Evans-Nguyen KM, Tolles LR, Gorkun OV, Lord ST, Schoenfisch MH. Interactions of thrombin with fibrinogen adsorbed on methyl-, hydroxyl-, amine-, and carboxyl-terminated self-assembled monolayers. Biochem 2005;44:15561–8.
[36] Gao JC, Li LC, Wang Y, Qiao LY. Corrosion resistance of alkali heat treated magnesium in bionics simulated body fluid. Rare Metal Mat Eng 2005;30(4):903–7.
[37] Alanazi1 AS, Hirakuri KJ. Blood compatibility of DLC films. Eur Cells Mater 2010;20(1):15–20.